Intake ground vortex and computational modelling of foreign object ingestion

D.G. MacManus
d.g.macmanus@cranfield.ac.uk
M. Slaby
Propulsion Engineering Centre
School of Aerospace, Transport and Manufacturing
Cranfield University
Cranfield
UK

ABSTRACT

When an aero-engine is operating on the ground the formation of a potent inlet ground vortex can arise which has the ability to ingest foreign object debris. The ingestion of foreign objects can cause notable damage to engine components as well as overall performance degradation. The assessment of foreign object ingestion has been conducted using a combination of computational fluid dynamics, analytical modelling and an Euler-Lagrange uncoupled discrete phase particle tracking method. The flow fields for a full-scale aero-engine have been simulated for a range of ground clearances and intake velocity ratios under crosswind conditions. The sensitivity of the debris ingestion thresholds and characteristics to particle size and material density has been evaluated. The characteristics of the ingestion location within the intake are also considered for a range of operating conditions and particle parameters.

NOMENCLATURE

Cp_{min}	minimum GV static pressure coefficient [-]	$\frac{p_{GVmin}-p_\infty}{0{\cdot}5\rho_i U_i^2}$
d_p	particle diameter [m]	
D_1	intake highlight diameter [m]	
E_k	kinetic energy [J]	
E_p	potential energy [J]	

Paper No. 4277. Manuscript received 20 October 2014, accepted 1 April 2015.

https://doi.org/10.1017/S0001924000011167 Published online by Cambridge University Press

F_{PS}	lift force acting on particle [N]
g	gravitational constant = 9·81 [ms^{-2}]
h	vertical distance from ground plane to the intake highlight BDC point [m]
H	vertical distance from ground plane to the engine centreline [m]
k	turbulent kinetic energy [Jkg^{-1}]
m_p	mass of the particle [kg]
p	static pressure [Pa]
p_{GVmin}	minimum static pressure in the GV core [Pa]
Q	particle weight [N]
r_c	GV radius [m]
r_c^*	non-dimensional GV radius r_c/r_l [-]
r_l	intake highlight radius [m]
r_p	particle radius [m]
Re_p	particle Reynolds number [-]
U	fluid velocity [ms-1]
U^*	velocity ratio U_i/U_∞ [-]
V	particle velocity [ms^{-1}]
V_{ini}	initial velocity of the particle [ms^{-1}]
x^*	non-dimensional axial position x/D_1 [-]
y^*	non-dimensional lateral position y/D_1 [-]
y^+	non-dimensional wall distance [-]
z_0	Terrain roughness length [m]

Greek symbols

Γ	vortex circulation [m^{2}s^{-1}]
Γ^*	non-dimensional circulation $\Gamma/(D_1U_i)$ [-]
ζ	the fraction of ingested particles [-]
ζ_{core}	the fraction of ingested particles into the engine core [-]
μ	dynamic viscosity [kgm^{-1}s^{-1}]
ν	kinematic viscosity [kgm^{-1}s^{-1}]
ρ_f	freestream fluid density [kgm^{-3}]
ρ_i	fluid density at the intake throat [kgm^{-3}]
ρ_p	particle density [kgm^{-3}]
τ	time scale [s]
ϕ	circumferential position on the engine fan face [°]
φ	yaw angle [°]
ω	specific turbulence dissipation rate [s^{-1}]

Subscripts

(x,y,z)	component aligned with (x,y,z) axis
∞	freestream conditions
c	GV core
i	intake throat
l	intake highlight
min	minimum magnitude
p	particle

https://doi.org/10.1017/S0001924000011167 Published online by Cambridge University Press

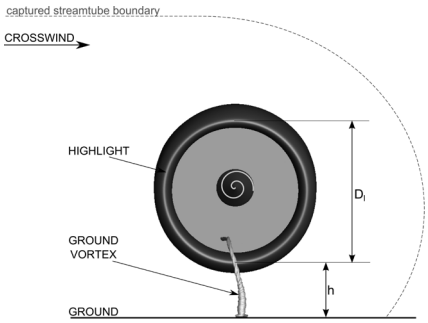


Figure 1. Schematic of captured streamtube interaction with ground resulting in a ground vortex. h/D_I = 0·40, U^* = 8·6 (U_∞ = 20ms^{-1}).

1.0 INTRODUCTION

When an aircraft is operating on the ground, there is a potential for the engines to ingest foreign object debris (FOD). It is well known that this foreign object ingestion (FOI) can result in notable engine damage and degradation as well as operating difficulties. For example, the costs incurred by airline operators in 2008 due to problems arising from FOI was estimated to be $12bn per year[1]. The likelihood of FOI arising clearly depends on a wide range of aspects including the engine operating condition, ambient conditions, engine intake design, position of the engine on the aircraft, and characteristics of the debris. Another key aspect for many aircraft configurations is the engine ground clearance as this has a strong influence on the nature of the local flow features and the intake aerodynamics. The development of civil aero-engine designs has demonstrated a general trend of reduced specific thrust requirements and increased bypass ratio which is usually associated with an increase in engine diameter. Consequently, there has been a concomitant trend for a reduction in engine ground clearance. In addition, some modern, wide-body, four-engine aircraft configurations result in the two outer engines positioned beyond the extents of typical paved runways. Accordingly, there is an increased likelihood of FOI since only the runway is scanned for potentially dangerous debris.

A year-long study for an airport showed that 60% of all FOD was made of metal[2]. Given that about 45% of identified debris was located on the taxiways and runways[1], where the aerodynamic interaction between the intake and the ground is the strongest, there is a clear possibility of ingesting potentially damaging material.

1.1 Ground vortices

When an intake operates in close proximity to the ground, there can be a notable interaction between the intake aerodynamics and the surface. The mechanisms and characteristics of ground vortices has been studied both experimentally[3-10] and computationally[11-13]. Overall these studies showed that the ground vortex can form under headwind, crosswind as well as quiescent conditions. The ground vortex formation process is based on the interaction of the intake captured streamtube with the ground plane and the potency of this interaction is affected by the approaching wind direction and approaching boundary layer (Fig. 1). In the context of practical aircraft operations, the vorticity is also affected by ambient gusts, other aircraft, buildings, and the fuselage which all combine to deteriorate the uniformity of the intake flowfield[14]. Although the ground vortex (GV) formation mechanism is complex[4,12], the formation threshold and vortex strength are predominately

https://doi.org/10.1017/S0001924000011167 Published online by Cambridge University Press

characterised by the ratio of intake throat velocity to ambient wind speed ($U^* = U_i/U_\infty$) and the clearance h/D_l, where h is a vertical distance between the intake lip and the ground and D_l is the intake highlight diameter (Fig. 1). A detailed experimental study of the GV characteristics using stereo particle image velocimetry quantified the vortex strength, size and location for a range of quiescent, headwind, and crosswind conditions[8,9,10,15]. These works quantified the GV strength as a function of U^*, h/D_l and yaw angle (φ) and identified that the crosswind operating conditions result in the GV with the greatest strength, the largest diameter and the most stability. Consequently, it was decided that this arrangement is a key concern for FOI and this current research focuses on crosswind configurations.

1.2 Ground vortices and FOI

Previous research has indicated that the presence of a GV depends on the formation of a ground stagnation point[4,14,16,17] where the ground vortex starts and extends to the inlet. The location of the stagnation point is generally unsteady such that the vortex footpoint wanders and so does the termination point at the fan face[18]. Under crosswind configurations the location of the vortex depends on U^* and h/D_l, and the GV is more stable than under headwind or quiescent conditions[8,9,15]. Although there have been a range of studies on ground vortices, the work of Murphy *et al*[15] is one of the few which has measured the detailed three-component velocity field of the GV. This work was performed using stereoscopic particle image velocimetry and determined the vortex flow modes, size, strength, and positions for a wide range of headwind, crosswind, and yawed configurations. The work of Ridder *et al*[18] measured the surface static pressure field associated with the GV for a number of configurations. Overall it was determined that the potency of the GV in terms of circulation and suction pressure coefficient was primarily affected by the flow yaw angle, ground clearance (H/D_i) and velocity ratio (U^*).

Computational studies have also been performed to assess the GV characteristics for a range of configurations including engine test cells[13] as well as for full aircraft configurations[19]. Zantopp[11] and Mishra[12] undertook a range of computational studies to simulate the experimental work of Murphy[8,9,15]. The work comprised both Reynolds averaged Navier-Stokes (RANS) and unsteady RANS simulations and encompassed a range of configurations for velocity ratio, ground clearance, and intake yaw angle. These studies identified some key aspects of the flow topology and detailed aerodynamics. It also showed that computational fluid dynamics (CFD) was able to successfully address this problem and overall good agreement was found between the experimental and the computational data.

Within the context of FOI, a particle on the ground which is located in proximity of the ground vortex footpoint will be affected by the vortex velocity and static pressure fields. There is the potential that the particle will first be moved by the GV and, in some cases, ingested by the engine. Current understanding of the ability of a ground vortex to lift and ultimately ingest FOD was developed using experimental studies[14,16,17,20]. Overall these investigations showed that FOI depends on the intake configuration, particle size, FOD material density and ground surface roughness. Along with these experimental investigations there has been some analytical work to develop an understanding of the fundamental underlying mechanisms by which the GV interacts with a particle on the ground[14,16,17,20].

The GV comprises a strongly three-dimensional flow field[8,9,15] which generates a notable static pressure reduction at the core of the vortex which affects the ground static pressure[11,18]. Consequently, it is expected that the particles on the ground will be exposed to the local static pressure field as well as the horizontal and vertical velocity field associated with the GV. A key aspect of the effect of the GV on the particle, and the possible subsequent ingestion, is the initial lift of the particle

https://doi.org/10.1017/S0001924000011167 Published online by Cambridge University Press

from the surface. It is envisaged that this is dominated by the effect of the suction force from the reduced static pressure at the GV core acting on the upper surface of the particle. The local flow accelerates over the particle upper surface and due to the stagnated flow on the underside, there is a vertical lifting force away from the ground plane[20]. The maximum lifting force is generated once the ground vortex stagnation point passes over the particle. In the situation where the particle lies within the ground vortex, but not at the exact core, an additional horizontal force will act on the particle due to the pressure difference between the front and rear surface and the lateral flow components[20].The resultant force can lift the particle off the ground and it was empirically shown that the lifting force acts as long as the particle is less than one radius above the ground[16]. In general, for particles which have a notable mass, after this initial movement, the particle follows a ballistic trajectory rather than that of the vortex core. If the initial force acting on the particles is high enough to project the particles into the captured streamtube and to direct them towards the inlet, then they may be ingested. Previous experimental work has shown that the likelihood of ingesting a particle is affected by the surface roughness of the ground plane[16]. It is reported that particles which are more embedded in the ground are more prone to be lifted into the air[16,20]. This is explained by a reduction in the local horizontal velocities acting on the particle as well as an increased resistance to the particle horizontal movement. Therefore the particle is less likely to get blown away in the horizontal plane and is more responsive to the vertical forces. Since the recommended airfield surface equivalent roughness is 1·5mm[21], there is the opportunity for particles of this scale to be effectively embedded in the surface and therefore to be more prone to ingestion. In addition, the particle density and size will clearly have an impact on the ingestion process. The size and shape of the particle will influence the magnitude of the aerodynamic forces whereas the density will influence the subsequent response and movement of the particle. Very small and very low density particles will have sufficient frequency response and modest drag to be able to follow the local flow gradients and will therefore broadly follow the air flow. In general, for these very small and light particles, although there is a high likelihood of being ingested, they are less likely to pose a threat to the engine. For a particle with a higher density, it will no longer follow the flow direction until at some level, for a given size, the particle will not move from the ground. Similarly, for a given density, there will be a size limit by which the lifting potential of the GV will be insufficient to cause the particle to move. In between these extremes there will be a range of particle sizes and densities which will be light enough to be affected by the GV but also of sufficient mass to be of concern to the engine.

Small objects, such as sand, are mostly responsible for clogging noise liners, combustion chamber and turbine cooling holes and contribute to the erosion of the leading edges of fan and compressor blades and compressor stator trailing edges. Medium and large objects, if lifted and directed into the engine, may damage inlet cowls and nacelle structures, and also significantly deteriorate fan blade leading edges[22]. Moreover, once lifted by a ground vortex, although not ingested by the engine there is a possibility of this debris affecting other components such as landing gears, tyres and flaps[23]. Apart from Rodert *et al*[20], all of the other experimental studies were carried out on model scale intakes in laboratory conditions. Although there is a growing importance to understanding FOI for current and future aero-engines, there is a severe lack of data and analytical models for full-scale configurations. This is not surprising given the difficulties in undertaking such experimental work and in getting quantitative data on the particle trajectories.

Along with assessing the impact of the GV on FOI, the aim of this research is to understand the sensitivities of the system and to determine the boundaries of the maximum particle sizes and mass that can be ingested. An additional aim is to understand the trajectory that is followed by the ingested particles and, in particular, if they are ingested into the engine core as this may result in significant engine damage.

https://doi.org/10.1017/S0001924000011167 Published online by Cambridge University Press

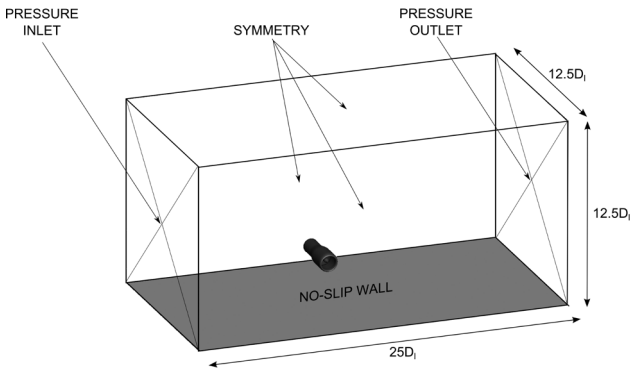


Figure 2. Computational domain size and boundary conditions.

2.0 METHODOLOGY

2.1 The computational domain

The geometry for the computational analyses was representative of a full-scale, modern high by-pass engine with a drooped and scarfed inlet with a 2·83m highlight diameter. The intake comprised a combined elliptical and NACA-1 section which had a non-uniform circumferential distribution of contraction ratio. The intake was positioned at a range of non-dimensional heights of $h/D_l = 0{\cdot}25$, 0·30, 0·40, and 0·80. The intake also contained a central non-rotating spinner which resulted in a maximum hub to tip ratio of 0·3 at the nominal fan face position which was located at $x/D_l = 0{\cdot}92$ from the highlight centre point. The intake duct extended as far as $x/D_l = 1{\cdot}47$ from the highlight centre point. The fan stage was not included in the configuration. The computational domain determined from previous studies[11] comprised a cuboid with the dimensions of $25 \times 12{\cdot}5 \times 12{\cdot}5D_l$ in the spanwise (Y), streamwise (X) and ground normal directions (Z), respectively (Fig. 2).

2.2 The boundary conditions

The side and top faces of the computational domain were specified as symmetry boundary conditions and the downstream face was set as a pressure outlet (Fig. 2). Previous work explored the sensitivity of the solutions to the domain size and boundary conditions and it was determined that this configuration was appropriate for these analyses[11]. The upstream boundary for the approaching crossflow was set as a pressure inlet condition, where the total pressure, total temperature, k, and ω profiles were specified. A fully developed full-scale boundary-layer velocity profile[24] was applied to the inlet face of the domain. To represent an airfield terrain with few trees and buildings a terrain roughness length (z_0) of 0·03m was prescribed based on the work of Hanses[25]. The required crosswind velocity magnitude was controlled by applying the appropriate total pressure at the inlet and keeping the outlet static pressure constant. The mass flow through the intake was regulated by applying a pressure outlet boundary condition which was controlled to deliver a specified mass flow. For all of the cases investigated here the intake mass flow was constant and set at 910kg/s. A key parameter was the non-dimensional velocity ratio ($U^* = U_i/U_\infty$) and this was controlled by adjusting the magnitude of ambient windspeed (U_∞).

https://doi.org/10.1017/S0001924000011167 Published online by Cambridge University Press

2.3 Computational method

The RANS formulation was used to determine the three-dimensional flowfield for a compressible, ideal gas. Viscosity was set using Sutherland's law. The k-ω shear stress transport (SST) turbulence model was used with wall-functions. Third-order monotonic upstream-centered scheme for conservation laws (MUSCL) was used for spatial discretisation. The solutions were converged to typically achieve residuals in the order of at least 10^{-4} and the iterative convergence was also considered by evaluating the variation in key parameters such as minimum static pressure. For a converged solution minimum static pressure convergence level was in the order of at least 10^{-5}.

Previous studies have examined the ability of CFD to calculate the key aerodynamic aspects associated with the ground vortex such as the vortex strength[11,12]. These studies showed that the vortex circulation was calculated within typically 13% of the measured data across a range of velocity ratios and flow yaw angles. It also showed that the CFD correctly determined the velocity ratio which resulted in the strongest GV circulation as well as highlighting that the characteristics were similar between model-scale and full-scale simulations. Overall this previous work concluded that CFD was capable of simulating the key aspects of the GV for these configurations. The current work is a continuation of these previous studies and follows the same computational methods, post-processing methods, procedures and strategies. Although there is no published quantitative experimental data available for FOI on full scale configurations, the previous validation of the underlying aerodynamic characteristics provides some confidence in the flow field simulations.

2.4 Grid sensitivity

The computational domain was discretised by using a hybrid mesh which used structured prism layers close to the ground plane and the intake surfaces as well as a region of tetrahedral elements in regions away from the walls. The near wall turbulence was modelled using a wall function and the grid was adjusted to give the appropriate values of y^+ for the k-ω SST model within the range of 30. The effect of the grid on the calculations was assessed by undertaking a grid sensitivity study with a range of hybrid grids comprising 6, 8, 10 and 13million cells. The y^+ was kept at the same level for each configuration. A range of key pertinent parameters were evaluated to quantify the effect of the grid resolution. The results presented in this paper are based on a final grid with approximately 8million cells. In terms of the position of the ground vortex footprint, the variation between the coarsest and the fine grids was found to be less than 1·0% in the y-direction and 1·2% in x-direction relative to intake highlight diameter. Overall the difference in GV location between the reported values and those from the finest mesh were less than 0·9%. The vortex strength was characterised in terms of the non-dimensional vortex strength ($\Gamma^* = \Gamma/(D_l U_i)$) and this increased by 2·6% from the coarsest to the finest mesh. The reported results are within 1·5% of the values calculated using the finest spatial resolution. The effect of the grid resolution on the particle ingestion characteristics has been considered for this similar range of mesh resolutions. For all particle material densities, the threshold size for the largest ingested particle changed by no more than 10% of r_p/r_l. Between the reported results and the finest mesh resolution, the local maximum of the ingestion fraction typically changed by less than 10%. Finally, as one of the main interests of the research is on the assessment of the impact of the GV on the ingestion of particles, this was evaluated by considering the potential lifting force by integrating the static pressure in the region of the calculated GV core. The reported values are within 10·5% of those calculated using the largest grid.

https://doi.org/10.1017/S0001924000011167 Published online by Cambridge University Press

2.5 Particle tracking

The particle tracking was performed using an uncoupled Euler-Lagrange approach to simulate a discrete second phase in a Lagrangian frame of reference. The foreign object particles were considered as a discrete phase affected by the working fluid and gravity, where each individual smooth spherical particle is treated as a point mass with a calculated drag which depended on the defined particle size and drag coefficient. The particles are assumed to be sufficiently sparse so that particle-particle interactions are neglected as well as the effect of the particles on the gas. Particles, treated as point masses, are released from a bounded square surface parallel to the ground and with an edge length equal to the vortex core diameter. The height of the surface over the ground varies with the particle size, and is equal to the particle radius r_p. This surface is always centred at the GV footpoint, such that the particle's initial position is restricted within the core. The initial position of the particles is the location of the computational grid points on the specified surface. Therefore, for the configurations investigated here, the number of particles released varies from 70 to 230. The number of ingested particles is non-dimensionalised by the number of the particles released and this ratio is defined as the fraction of particles ingested (ζ).

The particle tracking method requires an initial velocity V_{ini} to be specified as the initial lift force is not directly determined. The initial velocity was determined by calculating the lift force F_{PS} due to the local static pressure distribution from the CFD solution which was imposed on the upper surface of the spherical particle. The freestream static pressure was assumed on the particle underside[16]. The lift force was assumed to be constant and acting on the particle for a length of its radius r_p above the ground[16]. From energy conservation, work done by force F_{PS} over distance r_p is equal to the sum of potential energy, E_p , and kinetic energy, E_k, of the particle at this height (Equation (1)).

$$F_{PS}\, r_p = E_p + E_k \qquad \ldots (1)$$

Potential energy can be expressed as a negative integral of the gravity force acting on the particle, $m_p g$, from the ground up to the height r_p in the vertical direction Z (Equation (2)).

$$E_p = -\int_0^{r_p} m_p \vec{g}\, \mathrm{d}\vec{z} \qquad \ldots (2)$$

The energy of the particle due to its velocity V_{ini} is defined as a kinetic energy and the equation for non-rotating point mass m_p is shown in Equation (W3).

$$E_k = \frac{1}{2} m_p V_{ini}^2 \qquad \ldots (3)$$

Equation (1), (2), and (3) can be rearranged such that V_{ini} is given in a simple form:

$$V_{ini} = \sqrt{\frac{\left(2F_{PS} r_p\right) - \left(2m_p g r_p\right)}{m_p}} \qquad \ldots (4)$$

It is assumed that the particle drag can be neglected over such a short distance.

Once the particle is lifted, the motion of isolated particle in a flow field, known as Boussinesq-Basset-Oseen equation[26] can be expressed as follows:

https://doi.org/10.1017/S0001924000011167 Published online by Cambridge University Press

$$m\frac{\mathrm{d}V}{\mathrm{d}t} = \left[V\rho_f\left(\frac{DU}{Dt} - \mathrm{g}\right)\right]_I + [3\pi\mu d(U-V)]_{II} + \left[\frac{V}{2}\rho_f\left(\frac{DU}{Dt} - \frac{\mathrm{d}V}{\mathrm{d}t}\right)\right]_{III} + \left[\frac{3}{2}d^2\sqrt{\pi\rho_f\mu}\int_0^t\left(\frac{\frac{DU}{Dt} - \frac{\mathrm{d}V}{\mathrm{d}t}}{\sqrt{t-\tau}}\right)\mathrm{d}\tau\right]_{IV} + mg \quad \ldots (5)$$

where m is the particle mass, V particle velocity, ρ_f fluid density, U fluid velocity, g is the gravity acceleration, μ dynamic viscosity, and τ is a time-scale. The above equation is only valid when the particle diameter (d_p) is smaller than the local characteristic dimension. The term on the left hand side of the Equation (5) represents the change in the inertia of the particle. Term I in Equation (5) is the force in the undisturbed flow, produced by the pressure and shear stress gradient. Disturbed flow is represented by the next three terms: Stokes drag – II, virtual mass – III, and Basset gravity – IV. The last term is the body force caused by gravity. Equation (5) is valid for small particles at low particle Reynolds numbers $\mathrm{Re}_p \approx 1$. Re_p is defined as a ratio of particle inertial forces to viscous forces (Equation (6)):

$$Re_p = \frac{d_p(V-U)}{\nu} \quad \ldots (6)$$

where ν is a ratio of dynamic viscosity and fluid density. Clift *et al*[27] modified Equation (5) by adjusting the disturbed flow equation components for higher Reynolds numbers (Equation (7))

$$\left(1 + \frac{1}{2}\frac{\rho_f}{\rho_p}\right)\frac{\mathrm{d}V}{\mathrm{d}t} = \frac{3}{2}\frac{\rho_f}{\rho\rho_p}\frac{DU}{Dt} + \frac{18\mu}{\rho_p d^2}(U-V) + \left(1 - \frac{\rho_f}{\rho_p}\right)g + \frac{3}{\sqrt{2\pi}}\sqrt{\frac{\rho_f}{\rho_p}}\sqrt{\frac{18\mu}{\rho_p d^2}}\int_0^t\left(\frac{\frac{DU}{Dt} - \mathrm{d}}{\sqrt{t-\tau}}\right)\mathrm{d}\tau \quad \ldots (7)$$

For particles of a density considerably greater than the fluid density, by three or more orders of magnitude[27], Equation (7) reduces to:

$$\frac{\mathrm{d}V}{\mathrm{d}t} = \frac{18\mu}{\rho_p d^2}(U-V) + g \quad \ldots (8)$$

This is a typical equation representing motion of the heavy particles. Equation (8) is a first order linear differential equation thus the exact solution is given under assumption that the fluid velocity field is known.

2.6 Scope of configurations

A single nacelle and intake geometry was used throughout this study and the intake mass flow was kept constant. The intake ground clearance (h/D_l) was modified to span the range 0·25 to 0·8. The crosswind velocity was varied so that U^* ranged between 3 and 35 ($5\mathrm{ms}^{-1} \leq U_\infty \leq 57\mathrm{ms}^{-1}$). A range of particles with different densities and sizes were considered. Particle densities representative of sand ($\rho_p = 1{,}650\mathrm{kg/m}^3$), concrete ($\rho_p = 2{,}400\mathrm{kg/m}^3$), aluminium alloy ($\rho_p = 2{,}800\mathrm{kg/m}^3$), and steel ($\rho_p = 8{,}000\mathrm{kg/m}^3$) were evaluated and the particle size relative to the intake highlight radius (r_p/r_l) ranged from 0.00024 (r_p = 0·00034m) to 0·06 (r_p = 0·0849m). The Stokes number calculated just above the ground for all of the particles was always larger than 1.

https://doi.org/10.1017/S0001924000011167 Published online by Cambridge University Press

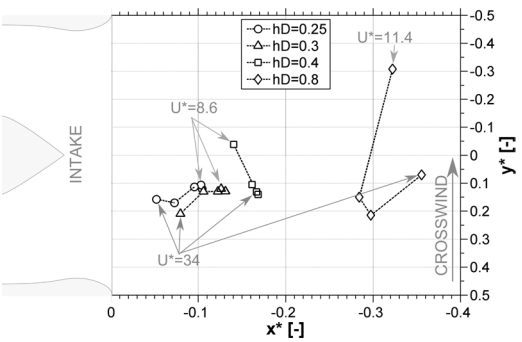


Figure 3. Ground vortex centre position as a function of velocity ratio (U^*) and ground clearance (h/D_l). Top view.

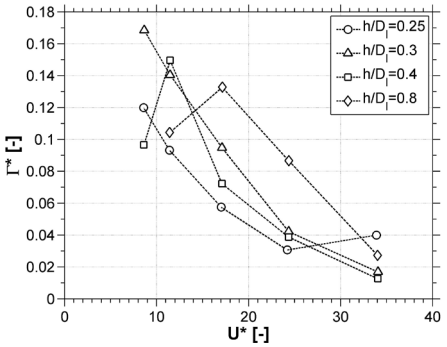


Figure 4. Non-dimensional circulation (Γ^*) as a function velocity ratio (U^*) and ground clearance (h/D_l).

3.0 RESULTS

3.1 Ground vortex characteristics

Although previous publications have assessed the details of the GV aerodynamics[8,9,11-13,15], it is of interest to consider some of these aspects within the context of GV and FOI. Of particular importance is the vortex strength, as characterised by Γ^*, the vortex position as well as the magnitude and extent of the local static pressure deficit at vortex core. The position and strength of the GV centre was evaluated at a height slightly above the ground plane ($z/D_l = 0{\cdot}0005$). Relative to the centre of the intake highlight plane the position of the GV primarily depends on the ground clearance (h/D_l) and the velocity ratio (U^*) (Fig. 3). In general, the GV moves further away from the highlight plane centre ($x^* = y^* = 0$) as the ground clearance increases and therefore the FOD has a greater path to follow before being ingested into the intake. In addition, when U^* is reduced by increasing the crossflow velocity (U_∞), the lateral position of the GV moves further downwind in the negative y^* direction.

At $h/D_l = 0{\cdot}40$ and $0{\cdot}80$, as U^* increases, the GV position moves further away from the intake (Fig. 3). Interestingly, the opposite behaviour takes place at lower ground clearances ($h/D_l = 0{\cdot}30$ and $0{\cdot}25$). Previous experimental work[3,7-10,15] has shown that the GV strength reaches a local maximum as U^* decreases until the GV rapidly loses strength and eventually does not form. These characteristics were also observed under the full-scale conditions investigated in this work where the configurations with h/D_l of $0{\cdot}40$ and $0{\cdot}80$ clearly show a local Γ^* maximum as a function of U^* (Fig. 4). The peak value of the GV strength increases as the h/D_l is reduced and the value of U^* at which the peak occurs also depends on the ground clearance, h/D_l (Fig. 4). For a lower ground clearance ($h/D_l = 0{\cdot}30$ and $0{\cdot}25$), the local maximum was not determined as the values of U^* were not extended into that regime which would have required a very high level of U_∞. Both the magnitude of the core static pressure reduction as well as the magnitude of the vortex local tangential velocity increase with the vortex strength and these will have an impact on the particle initial velocity and trajectory.

The minimum static pressure which arises at the footprint of the GV is affected by the vortex strength which impacts on the ability of the GV to lift the particles from the ground. The minimum static pressure coefficient has some characteristics which are similar to the GV strength such as

https://doi.org/10.1017/S0001924000011167 Published online by Cambridge University Press

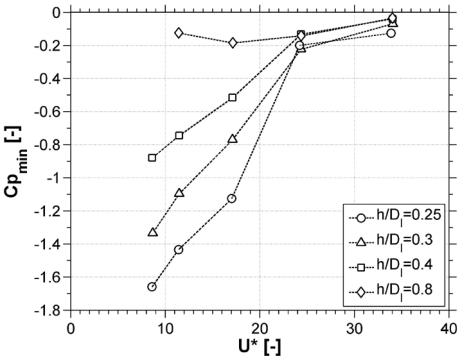


Figure 5. Minimum static pressure coefficient (Cp_{min}) as a function velocity ratio (U^*) and ground clearance (h/D_l).

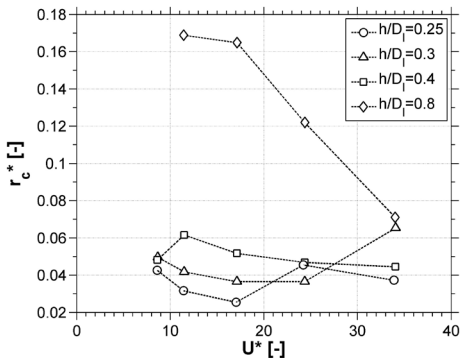


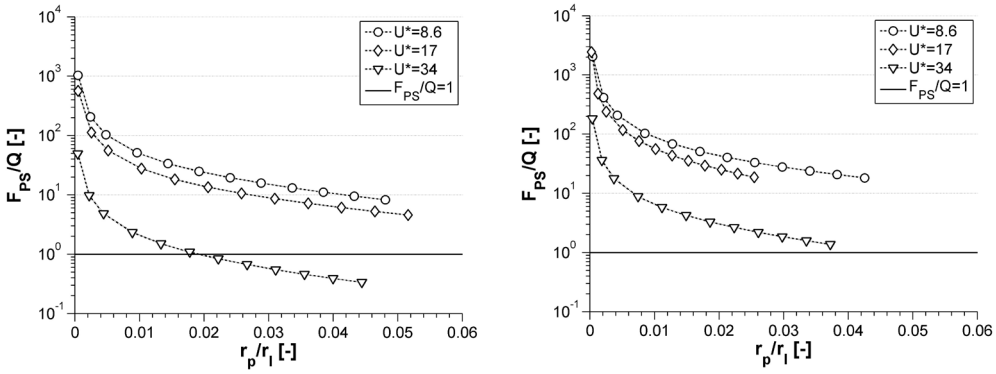
Figure 6. Ground vortex core radius (r_c^*) as a function velocity ratio (U^*) and ground clearance (h/D_l).

the magnitude of Cp_{min} increases as U^* decreases (Fig. 5). Although not visible on Fig. 5 there is a local minimum of Cp_{min} for all of the ground clearances at very low U^* representative of a very strong U_∞. For all cases, the magnitude of Cp_{min} reduces as U^* decreases and as the sucked streamtube eventually lifts away from the ground plane the GV does not form. Similar to the Γ^* characteristics, the magnitude of Cp_{min} continues to increase for the configurations with the lowest ground clearance (h/D_l = 0·30, 0·25). It is also notable that there are relatively large changes in Cp_{min} across this range of configurations. For example, the strongest suction (Cp_{min}) for h/D_l of 0·40 is approximately –0·88, whereas when h/D_l is reduced to 0·25, the magnitude of Cp_{min} increases to approximately –1·66. Consequently it is envisaged that this will have a notable influence on the particle response to the GV flow field.

3.2 Initialisation of particle lifting

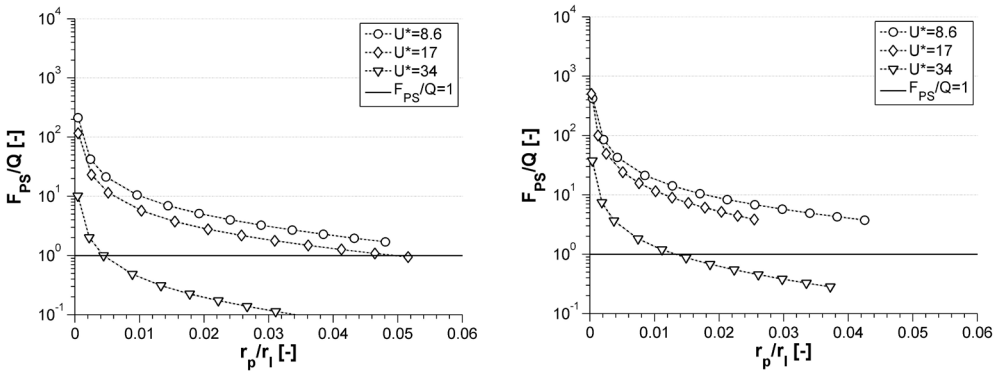
The initial lifting of the particles from the ground is considered in terms of the suction force on the particle (F_{PS}) due to the static pressure deficit at the vortex core relative to the gravitational force (Q) which depends on the particle size and density. There is a possibility that the particle will move away from the surface when the ratio of F_{PS}/Q is greater than 1 although the sensitivities of this threshold depend on the GV characteristics which in turn depends on h/D_l and U^*. For a given particle density, there are the competing elements of the change in lift force (F_{PS}) which increases proportionally to r_p^2 whereas the gravitational element (Q) increases with r_p^3. These aspects have been considered for a range of GV configurations as well as particle sizes (r_p/r_l) and material density (ρ_p). For the configuration of h/D_l = 0·40 (Fig. 7(a)) the lifting ratio, F_{PS}/Q, reduces monotonically as the particle size increases across the range of U^* from 8·6 to 34 (U_∞ from 20ms^{-1} to 5ms^{-1}). However, there is a notable reduction in F_{PS}/Q for the higher U^* of 34 (U_∞ = 5ms^{-1}). This is because at this velocity ratio there is a large reduction in the GV static pressure coefficient (Fig. 5) and eventually for particles with r_p/r_l greater than 0·018 (r_p > 0·0255m) the lifting criteria F_{PS}/Q is less than 1 and there is insufficient suction to lift the particle (Fig. 7(a)). When the ground clearance is reduced to h/D_l of 0·25, there is an increase in the magnitude of Cp_{min} (Fig. 5) so that even at a relatively high velocity ratio of U^* = 34 (U_∞ = 5ms^{-1}), all of the particles now have an F_{PS}/Q greater than the critical value of 1 (Fig. 7(b)). Although this is a simplified model, it is of interest to develop an understanding of the potential lifting force that is generated within the vortex core. For example, considering the case with h/D_l of 0·25 and U^* of 8·6 (U_∞ = 20ms^{-1})

https://doi.org/10.1017/S0001924000011167 Published online by Cambridge University Press



(a) h/D_l = 0·40 (b) h/D_l = 0·25

Figure 7. Suction (F_{PS}) to gravitational (Q) force ratio for sand particles (ρ_p = 1,650kg/m^3).



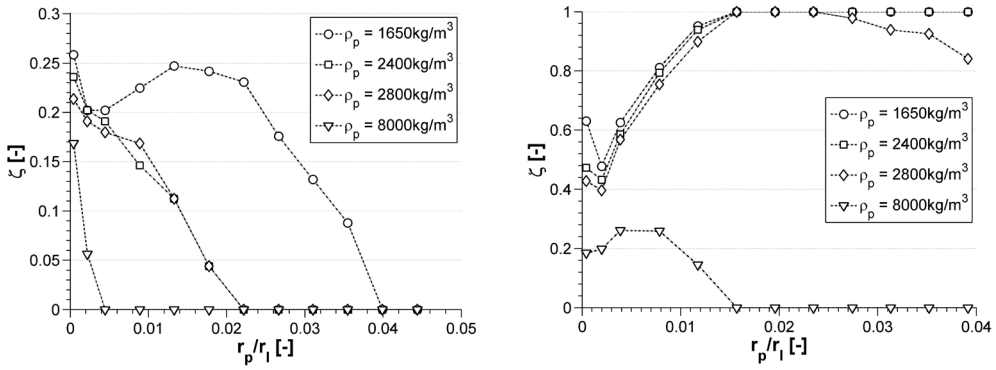
(a) h/D_l = 0·40 (b) h/D_l = 0·25

Figure 8. Suction (F_{PS}) to gravitational (Q) force ratio for steel particles (ρ_p = 8,000kg/m^3).

the Cp_{min} is approximately –1·66 (Fig. 5). For this case the GV core size of r_c/r_l is approximately 0·042 (Fig. 6) which for the full-scale geometry evaluated here is a radius 59mm. Considering the limiting case of a uniform static pressure distribution across the vortex core this equates to a maximum local lifting force of approximately 287N and a potential object of approximately 29kg.

Particles of greater density generally follow a similar pattern as that of light sand particles presented in Fig.7. The F_{PS}/Q ratio reduces monotonically with particles size for both ground clearances (Fig. 8), but the magnitude of the suction force to weight ratio (F_{PS}/Q) is significantly reduced due to the increase in particle density. For the high ground clearance case (h/D_l = 0·40) (Fig. 8(a)) at the highest U^* = 34 (U_∞ = 5ms^{-1}) only particles that are smaller than r_p/r_l = 0·004 are lifted. At the same crosswind speed (U^* = 34, U_∞ = 5ms^{-1}) but lower ground clearance (h/D_l = 0·25)(Fig. 8(b)) the maximum size of the particle that can be lifted is increased to r_p/r_l = 0·012 due to a significant increase in the Cp_{min} (Fig. 5).

https://doi.org/10.1017/S0001924000011167 Published online by Cambridge University Press



(a) h/D_l = 0·40, U^* = 8·6 (U_∞ = 20ms^{-1}) (b) h/D_l = 0·25, U^* = 8·6 (U_∞ = 20ms^{-1})

Figure 9. Ingestion fraction (ζ) as a function of particle size (r_p/r_l) for a variety of particle densities.

3.3 Effect of particle size and mass on ingestion characteristics

The previous section identified the sensitivities of the initiation of a particle motion by the GV and the effect of the particle size and material density on the balance of the lifting force and particle weight. The ingestion of particles of a variety of sizes and densities highlights a variety of mechanisms and aspects which affect FOI. For example, for sand particle (ρ_p =1,650kg/m^3) with an intake configuration of a medium ground clearance (h/D_l = 0·40) and a very low velocity ratio (U^* = 8·6, U_∞ = 20ms^{-1}), where the magnitude of Cp_{min} is relatively large (Fig. 5), the fraction of particles (ζ) that are ingested depends on the particle size (Fig. 9(a)). For very small sand particles, although the F_{PS}/Q is substantially greater than 1 and the particles are lifting from the surface, a relatively low fraction (approximately 26%) is ingested. This is because subsequent to the particles being lifted from the surface, they have a sufficiently low mass so that they are moved out of the vortex trajectory and eventually are blown away downstream and not ingested (Fig. 9(a)). Interestingly, an increase in the particle size from r_p/r_l = 0·0004 to 0·005 results in a small reduction in the ingestion fraction. The initial trajectory of the particle is affected by the GV tangential velocity to the similar extent as for smaller particles. However, due to the higher particle inertia it takes more time for the captured streamtube and crosswind to change the particle trajectory and direct it into the intake. As the particle mass further increases with size (r_p/r_l), there is still a sufficient lifting force (F_{PS}/Q > 1) but now the particles follow a different trajectory so that more of the particles are ingested (ζ = 0·25) (Fig. 9(a)). However, as the particle size increases further beyond r_p/r_l > 0·02, there is a monotonic reduction in the ingestion fraction. This is due to the associated reduction in F_{PS}/Q which, although still greater than 1, results in a lower initial velocity and ultimately a different ingestion fraction. Eventually at r_p/r_l of 0·04 (r_p = 0·0566m), and with a decreasing F_{PS}/Q, there are no particles ingested.

Broadly similar characteristics are also observed when concrete and aluminium particles with a material density of 2,400kg/m^3 and 2,800kg/m^3 are considered (Fig. 9(a)). In this case the effect of the increased particle mass is to reduce the maximum ingestion fraction down to approximately 0·24 with a more rapid decrease in ζ with increasing r_p/r_l. In addition, the threshold at which ζ reaches zero reduces from 0·04 for sand (ρ_p = 1,650kg/m^3) to 0·022 for concrete and aluminium (ρ_p = 2,400-2,800kg/m^3). Finally, when there is a more substantial increase in the material density to that of steel (ρ_p = 8,000kg/m^3), it is only for a very small

https://doi.org/10.1017/S0001924000011167 Published online by Cambridge University Press

range of particle sizes that any ingestion arises. Even then, the ingestion fraction is very small at approximately 0·17 and reaches 0 when r_p/r_l is greater than 0·004. However, it is also of interest to note that the initial lift criteria of F_{PS}/Q is still greater than 1 (F_{PS}/Q = 27·1), but that the particles are not ingested.

3.4 The effect of ground clearance on ingestion characteristics

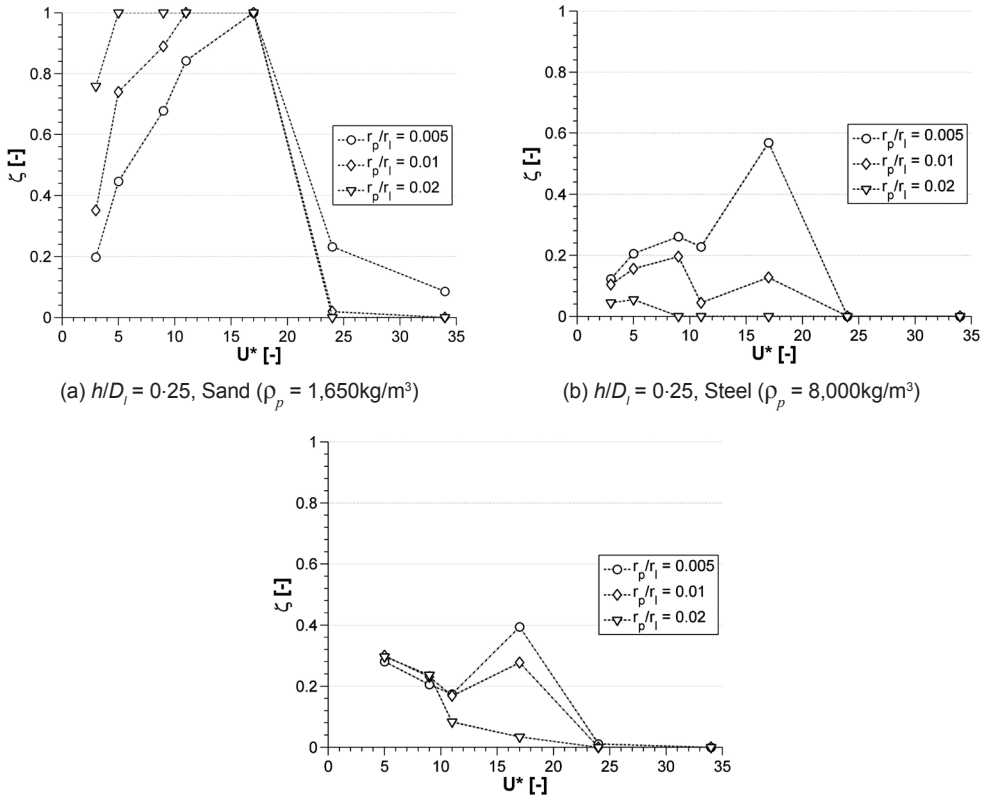
Although the main effects of particle size and density on the ingestion characteristics are of key interest, the sensitivity to the ground clearance (h/D_l) and velocity ratio (U^*) are also expected to have a first-order effect as these two parameters drive the pressure deficit in the GV core, the vortex size and the flow conditions around the intake. For example, at the velocity ratio of U^* = 8·6 (U_∞ = 20ms^{-1}) and low ground clearance (h/D_l = 0·25), the magnitude of minimum static pressure coefficient is approximately twice as large as that at h/D_l = 0.40 (Fig. 5). At the same time the radius of the GV is comparable (Fig. 6).

In comparison with the datum configuration (h/D_l = 0·40, U^* = 8·6 Fig. 9(a)), for the case with a lower ground clearance (h/D_l = 0·25) there is a notable change in the ingestion fractions (Fig. 9(b)) for an entire range of sizes of sand (ρ_p =1,650kg/m^3), concrete (ρ_p =2,400kg/m^3), and aluminium particles (ρ_p =2,800kg/m^3). At this lower h/D_l the ingestion fraction still depends on the particle size with ζ values of up to 1·0 for the sand, concrete and aluminium particles. Although this is a large change in ζ, there are some similarities with the ingestion characteristics at h/D_l =0·40. For example, for the sand, concrete and aluminium particles, the distribution of ζ with r_p/r_l is non-monotonic with a small local minimum at r_p/r_l = 0·002 where there is a change in the trajectory of the particle once it is lifted from the surface. In addition, as also observed at h/D_l = 0·40, as ρ_p increases it eventually begins to impact on the ingestion fraction so that for ρ_p = 2,800kg/m^3 when r_p/r_l is greater than about 0·024 the ingestion fraction reduces from 1·0 to about 0.84 (Fig. 9(b)). This highlights that although ζ increases for a reduced h/D_l the particles are still highly sensitivity to the vortex tangential velocity component. Once lifted above the ground and moved away from the vortex core, the particle trajectory is once again easily changed by the crosswind and captured streamtube. As the particle size increases above r_p/r_l = 0·002, the GV tangential velocity effect on the particle trajectory reduces significantly until it has a minimal influence and all of the particles are ingested. Although F_{PS}/Q reduces when the particle size increases, there is still enough suction force to lift and ingest all of the largest particles (r_p/r_l = 0·039).

At h/D_l = 0·25, for the more dense steel particles (ρ_p =8,000kg/m^3) the ingestion fraction is relatively low but still larger than that at the higher ground clearance of h/D_l = 0·40. The smallest of the steel particles are ingested with a ζ of about 0·20, even though F_{PS}/Q is approximately 550 Fig. 8(b). Further increase in particle size leads to a small increase in the number of ingested particles due to higher particle inertia and the smaller effect of GV tangential velocity. The maximum fraction of 0·28 is reached for the steel particles of r_p/r_l = 0·005 (r_p = 0·0071m). Above this size the F_{PS}/Q drops significantly, but is still greater than 1 (Fig. 8(b)), and the particles do not have enough vertical velocity to reach sufficient height and to be ingested. The ingestion fraction decreases monotonically until the particle size is r_p/r_l = 0·016 and larger particles are not ingested.

In addition to understanding the sensitivity of the ingestion fraction to the ground clearance, particle size and particle density, these results also highlight the important finding that the previously reported minimum particle lifting criteria (F_{PS}/Q > 1) is insufficient to identify a boundary for which ingestion occurs.

https://doi.org/10.1017/S0001924000011167 Published online by Cambridge University Press



(a) h/D_I = 0·25, Sand (ρ_p = 1,650kg/m^3)

(b) h/D_I = 0·25, Steel (ρ_p = 8,000kg/m^3)

(c) h/D_I = 0·40, *Sand* (ρ_p = 1,650kg/m^3)

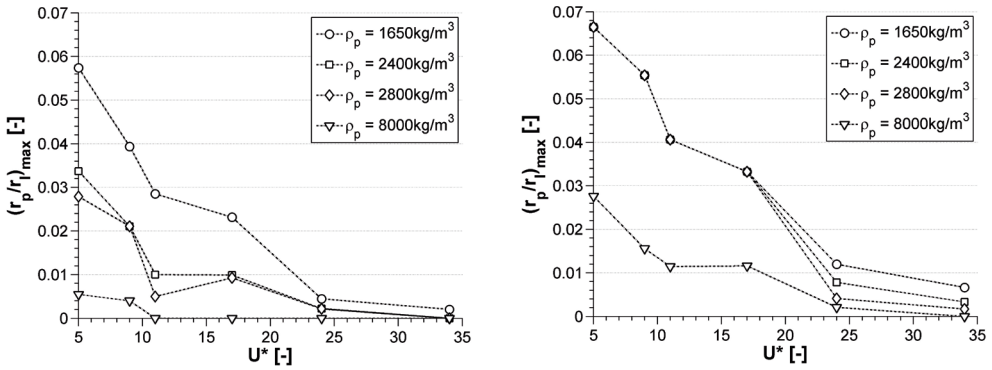
Figure 10. Ingestion fraction (ζ) as a function of velocity ratio (U^*) for a variety of particle sizes (r_p/r_I) and particle densities (ρ_p).

3.5 The effect of velocity ratio on ingestion characteristics

The velocity ratio U^* is expected to have a key role in FOI as it influences both the vortex static pressure footprint as well as vortex circulation and the vortex tangential velocity. The minimum vortex static pressure increases in magnitude as U^* reduces until a local suction maximum is usually reached (Fig. 5). This behaviour is also reflected in the F_{PS}/Q distribution (Fig. 7) for both ground clearances, where F_{PS}/Q increases with reducing U^*. Further U^* reduction leads to the GV being blown away and no more static pressure drop is available in the GV core. Equally, the freestream captured streamtube properties are affected by the velocity ratio. Assuming that intake mass flow is constant and the crosswind speed is varying, at low U^* the particle is impelled into the strong crosswind environment that has a significant effect on the trajectory. On the other hand, when U^* is high, crosswind speed is relatively low and has little or no effect on the particle path. To demonstrate the effect of velocity ratio on the ingestion of particles, sand (ρ_p = 1,650kg/m^3) and steel (ρ_p = 8,000kg/m^3) particles of different sizes are considered.

Regardless of size, the ingestion fraction of sand (ρ_p = 1,650kg/m^3) particles broadly varies in a similar manner (Fig. 10(a)). At a very low velocity ratio (U^* = 3, U_∞ = 57ms^{-1}) only 20% of the smallest particles is ingested. Despite that the lifting-weight ratio F_{PS}/Q is significantly larger than

https://doi.org/10.1017/S0001924000011167 Published online by Cambridge University Press



(a) h/D_l = 0·40 (b) h/D_l = 0·25

Figure 11. Maximum size (r_p/r_l) of ingested particles as a function of velocity ratio (U^*) for a variety of particle density.

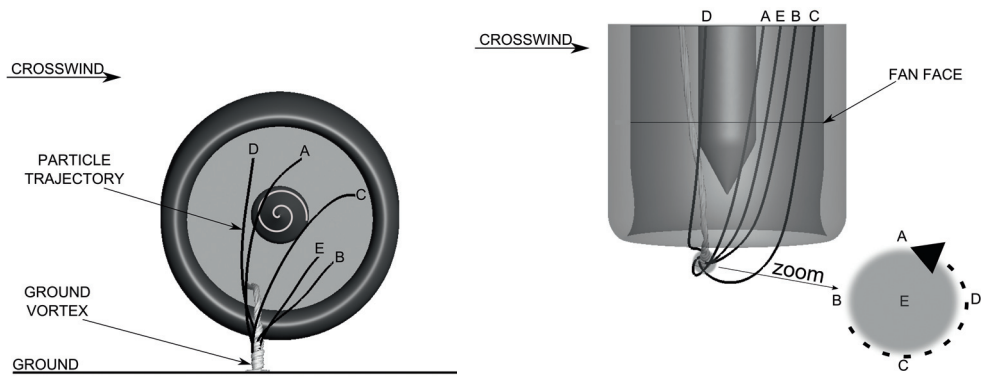
1, the high crosswind results in a substantial drag on the particle which blows the particle away from the intake and avoids ingestion. The ingestion fraction of larger particles (r_p/r_l = 0·02) is much higher at U^* = 3 (U_∞ = 57ms^{-1}) due to the particle higher initial inertia and, as a consequence, less sensitivity to the crosswind. A further increase in U^* results in a greater number of particles being ingested. At U^* = 17 all of the smallest particles (r_p/r_l = 0·005) are ingested. Although a ζ = 1 for larger particles is achieved for lower U^*, there is a minimum U^* = 17 common for all particle sizes after which a further increase in velocity ratio results in a sudden drop of ζ. The results indicates that the ingestion fraction of larger particles is higher over a wider range of velocity ratios. Although contrary to perhaps initial consideration, large particles are more prone to be ingested and are a greater threat to the engine operability. These results also highlight that although there is a relationship between the vortex strength and the ingestion fraction, it is a more complex process which also depends on the relative size and density of the particles.

As expected when the particle density is increased to ρ_p = 8,000kg/m^3 there is a notable reduction in ζ (Fig. 10(b)). The largest of the steel particles (r_p/r_l = 0·02) are only ingested at low U^* < 8·6 due to the high particle mass. The ingestion fraction of smaller particles reaches two local maxima at U^* = 8·6 and U^* = 17. This is due to two related characteristics that are driven by U^*, namely the GV strength and the crosswind flow velocity. However, once the velocity ratio is higher than 17 no ingestion occurs. At higher ground clearance (h/D_l = 0·40), the ζ variation with U^* is similar to steel presented in Fig. 10(b) with two local maxima (Fig. 10(c)).

3.6 The maximum size of the ingested particle

In addition to the effect of the particle size and mass on the ingestion fraction, it is of interest to evaluate the maximum particle size that could potentially be ingested. Although the initial lifting condition based on $F_{PS}/Q > 1$ is a useful initial criteria, it does not capture the aspects of whether the particle is actually ingested. For a ground clearance of h/D_l = 0·40, the maximum particle size (r_p/r_l) that is ingested is considered for a range of U^* and particle material density (ρ_p) (Fig. 11(a)). In general, the maximum ingested particle size decreases as U^* increases (Fig. 11(a)) and the maximum particle size reduces as ρ_p increases. However, the changes in $r_{p\,max}$ do not change linearly with ρ_p. In addition, the reduction in $r_{p\,max}$ with U^* is not monotonic for all cases. For

https://doi.org/10.1017/S0001924000011167 Published online by Cambridge University Press



(a) view at the nominal fan face plane (b) top view

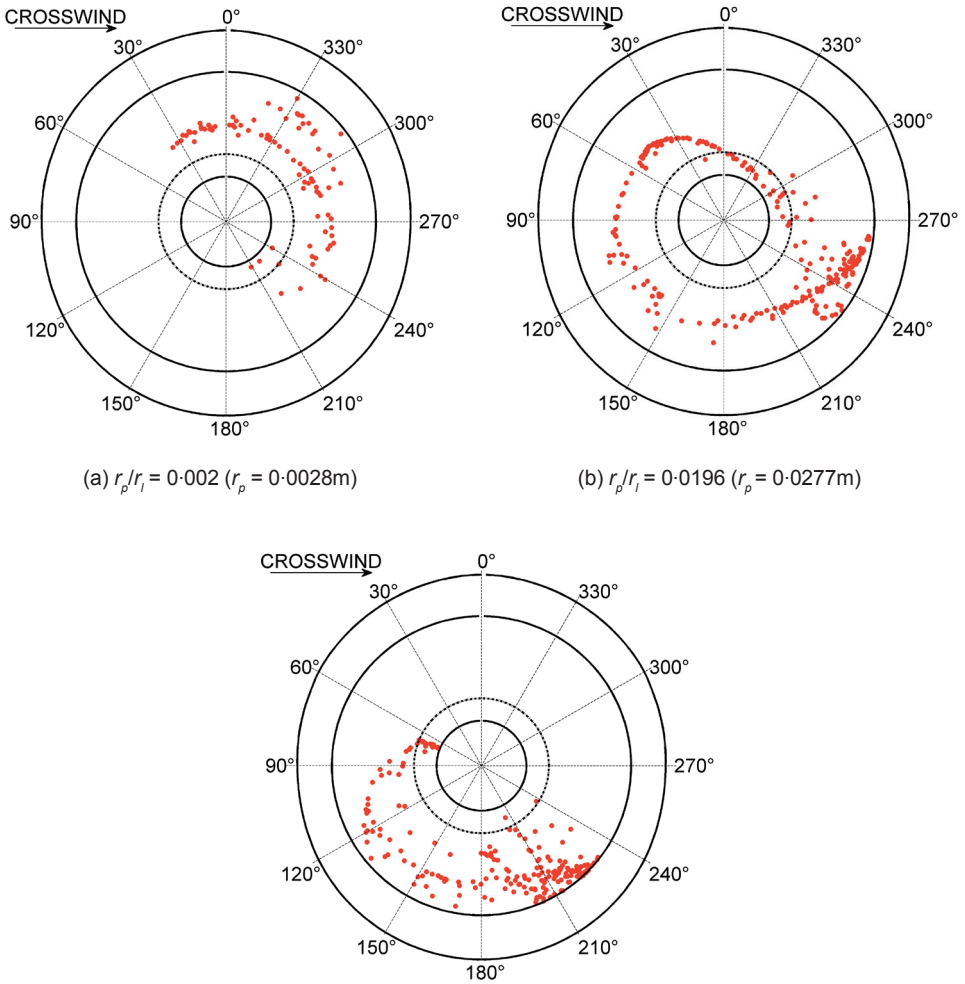
Figure 12. Sand particles trajectories under crosswind U^* = 8·6 (U_∞ = 20ms^{-1}), h/D_l= 0·25 (ρ_p =1,650kg/m^3, r_p/r_l = 0·038, r_p = 0·0538m).

this ground clearance (h/D_l = 0·40), when the materal is changed to steel (ρ_p = 8,000kg/m^3) there is a notable drop in the maximum particle size to r_p/r_l = 0·005. For a lower ground clearance of h/D_l = 0·25, it is established that the magnitude of Cp_{min} increases across the range of U^* (Fig. 5) and there is also an increase in the size of the particle that is ingested. This is of particular significance for the steel particles where the maximum particle size is approximately 0·01 across the range of U^* from 11 to 17 (Fig. 11(b)). At the lowest velocity ratio (U^* = 5) the maximum steel particle of r_p/r_l = 0·028 weights approximately 2kg. For the lower ground clearance (h/D_l = 0·25) and velocity ratio of U^* < 24 the maximum ingested particle size for sand, concrete, and aluminium exceeded the size of the ground vortex core and due to the limititation of the method, the maximum particles size at low U^* was not evaluated. The maximum size for these matierials for U^* < 24 shown on Fig. 11(b) represents the size of the ground vortex core and is considered as the maximum ingested size.

3.7 Ingestion mechanism

Although the GV can be a prime mover in terms of FOI, the exact mechanisms of the ingestion process are not fully understood. Some of the previous studies, using model-scale configurations[14,16,17], reported that the particles usually do not follow the vortex path and indeed in certain circumstances the particles are initially lifted from the surface by the GV, but then are subsequently blown downstream and ultimately not ingested[16]. It is expected that the particle then moves mainly under the influence of gravity and the friction with the freestream air but with its surface providing no significant lift to modify the course of flight[16]. Particles located closest to the intake highlight, point A in Fig. 12, are most likely to be ingested as these are mainly influenced by the GV tangential velocity component that opposes the crosswind. Particles positioned close to points B and C are blown away as the vortex initially directs them away from the intake highlight. For the particle impelled from the GV centre (point E) the velocity tangential component has little or no effect on the trajectory. Once the particle has lifted sufficiently it is blown downwind by the effect of the crossflow until the influence of the inlet captured streamtube is strong enough to affect the trajectory. Overall the particle typically does not follow the path of the GV and the trajectory is strongly dependent on the initial position relative to the vortex core (Fig. 12).

https://doi.org/10.1017/S0001924000011167 Published online by Cambridge University Press



(a) r_p/r_l = 0·002 (r_p = 0·0028m)

(b) r_p/r_l = 0·0196 (r_p = 0·0277m)

(c) r_p/r_l = 0·0392 (r_p = 0·0555m)

Figure 13. Ingestion position on the fan face as a function of particle size (r_p/r_l) for aluminium (ρ_p = 2,800kg/m^3). Ground clearance of h/D_l = 0·25 and velocity ratio of U^* = 8·6 (U_∞ = 20ms^{-1}). View looking at the fan.

3.8 Ingestion distribution

The likely effect of the particle ingestion will also depend on the ingestion location and, in particular, if the FOD is ingested into the engine core, the fan tip or down the bypass duct. The results in Fig. 9 indicate that the eventual ingestion of a particle depends on a range of parameters and mechanisms which is also reflected in the distribution of particles at the intake fan face (Fig. 13). For example, with a low ground clearance (h/D_l = 0·25), there is a medium ingestion fraction (ζ = 0·4) for small particles and this is also reflected in the fan face ingestion distribution where these small particles (r_p/r_l = 0·002) are mostly ingested around the upper

https://doi.org/10.1017/S0001924000011167 Published online by Cambridge University Press

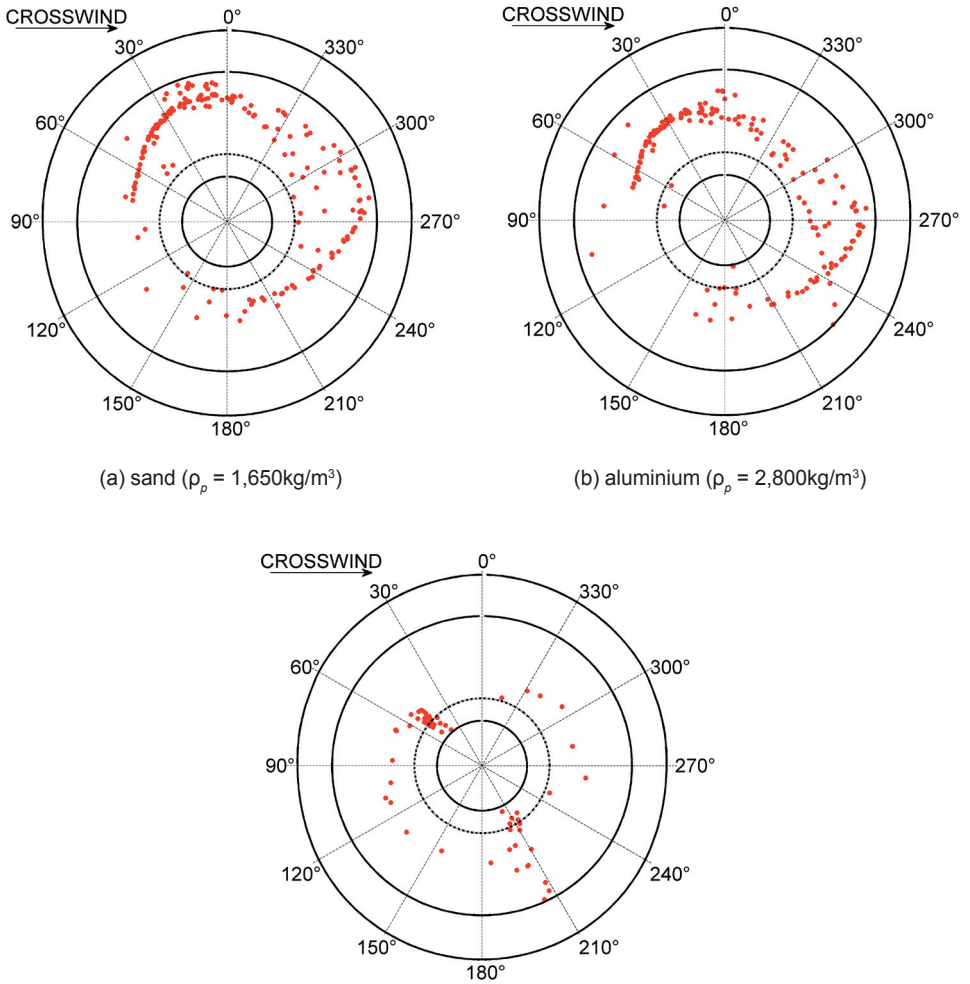
right quadrant (φ = 270° to 360°). The other particles are not ingested as they pass outside of the sucked streamtube on the downwind side. For medium sized particles (r_p/r_l = 0·0196), the ingestion fraction is 1.0 and the influence of the crosswind velocity is reduced where there is a wider distribution across the full nominal fan face plane with particles ingested at all circumferential positions (Fig. 13(b)). However, when the particle size increases to approximately r_p/r_l = 0·0392, the particle mass begins to dominate, the ingestion fraction is slightly reduced to 0·84 and the ingestion location is predominantly in the sectors closer to the ground (φ = 90° to 240°).

The two outer circular lines in Fig. 13 are representative of the nacelle external and internal edges at the fan face axial position. The circle of the smallest radius represents the spinner at the fan face. For the purpose of this analysis it was assumed that the engine bypass ratio is 7, based on a class of current in-service engines. Assuming uniform velocity and density across fan face, the core radius was calculated to be $r_{core} = 0{\cdot}45r_{fan}$ and is presented as a dotted circular line (Fig. 13). The simplified criterion of particle ingestion into the core model is based on the assumption that any particles located radially inside the core radius (r_{core}) will be ingested into the core. However, before the core inlet is reached, the ingested particle has to travel through the rotating fan blade set and therefore the reported core ingestion fraction (ζ_{core}) is just an indication of ingestion location. The core ingestion fraction (ζ_{core}) is defined as a ratio of the number of particles ingested to the total number of particles released. For small particles only a small fraction (ζ_{core} = 0·02) (Fig. 13(a)) is ingested into the core. The ζ_{core} increases significantly with the particles size (Fig. 13(b)) where approximately 11% of all medium sized particles (r_p/r_l = 0·0196) are ingested within the core radius. A further increase in the particle size to r_p/r_l = 0·0392 (Fig. 13(c)) results in a slight reduction in ζ_{core} to 0·07 and therefore for a given particle density, there is a specific particle size that is more likely to be ingested into the engine core.

3.9 The effect of the particle material density on distribution

The effect of the density of the particle density (ρ_p) on the distribution at the nominal fan face is considered for low ground clearance (h/D_l = 0·25) and a relatively strong crosswind (U^* = 8·6) (Fig. 14). For these medium sized particles with r_p/r_l = 0·008 the ingestion fraction varies with density (Fig. 9(b)), such that 81% of sand (ρ_p = 1,650kg/m^3) and 75% of aluminium (ρ_p = 2,800kg/m^3) particles are ingested. The relatively small effect of the sand and aluminium particle density can be seen in the fan face distribution (Fig. 14). For both densities a wide region across the face is covered with a notably reduced population in the lower left quadrant of φ = 90° to 180°. There is a minor difference in radial distribution of the particles as the greater mass of the aluminium particles, and therefore lower F_{PS}/Q ratio, results in ingestion at a reduced maximum radius. For example, the sand particles from the fan face top region, φ = 330° to 30°, are positioned at approximately 75% of the blade height. The increase in the particle density for aluminium, moves the radial ingestion position towards a more inboard region of the blade height. This effect is more noticeable when the particle density is almost tripled to ρ_p = 8,000kg/m^3. For these steel particles, the ingestion fraction reduces to ζ = 0·26. There are two regions on the fan face φ = 30° to 90° and 180° to 240° where the majority of the particles are ingested. In comparison to the sand particles (ρ_p = 1,650kg/m^3), the ingestion position for steel particles is generally offset vertically downwards towards the ground relative to the sand and aluminium distributions. Clearly in this case the effect of the particle mass on the F_{PS}/Q ratio, the concomitant initial velocity, and the effect of gravity has a notable impact on the trajectory and the basic aerodynamic drag on these particles of the same size will be similar.

https://doi.org/10.1017/S0001924000011167 Published online by Cambridge University Press



(a) sand (ρ_p = 1,650kg/m^3)

(b) aluminium (ρ_p = 2,800kg/m^3)

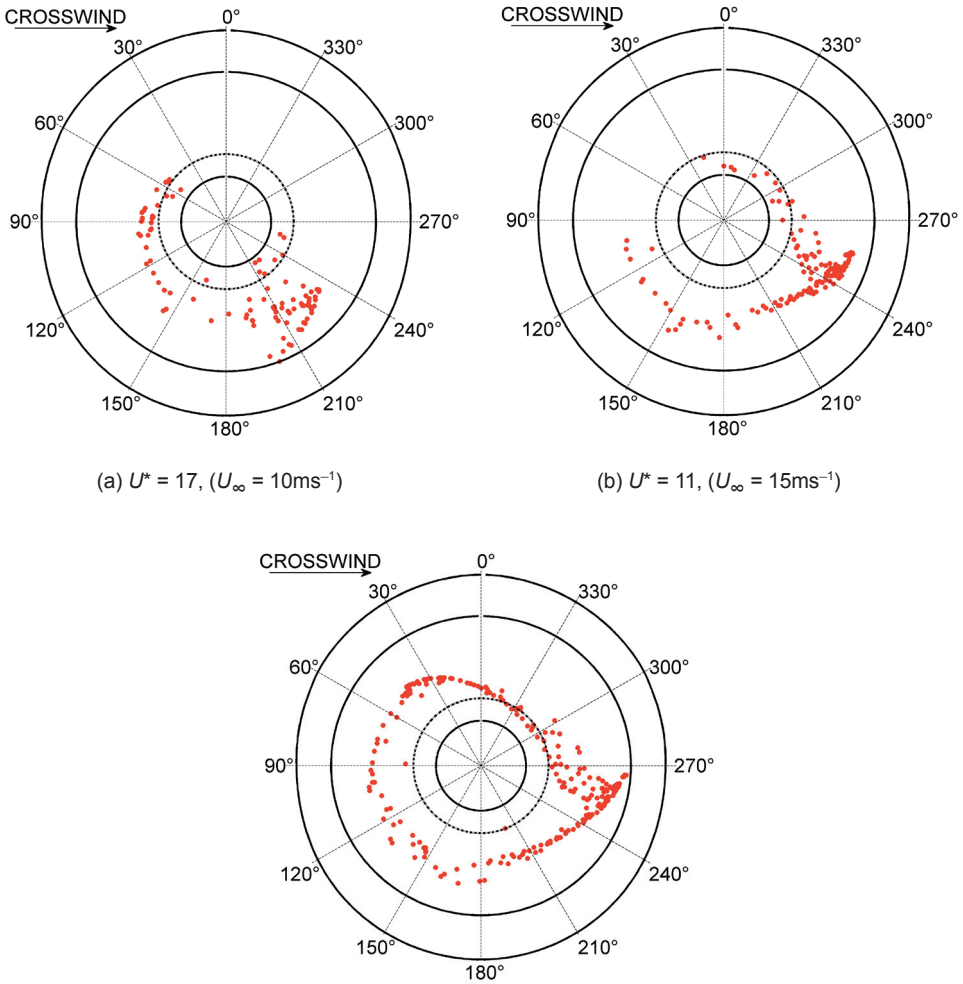
(c) r_p/r_l = 0·0392 (rp = 0·0555m)

Figure 14. Ingestion position on the fan face as a function of particle density (ρ_p) for the same size particle (r_p/r_l = 0·008, r_p = 0·0113m). Ground clearance of h/D_l = 0·25 and velocity ratio of U^* = 8·6 (U_∞ = 20ms^{-1}). View looking at the fan.

3.10 The effect of velocity ratio on foreign object distributions

The GV size and strength depends on the velocity ratio U^*, which for a fixed intake mass flow decreases with stronger crosswind. The increase in the crosswind velocity changes the size of the captured streamtube, the ingested and generated vorticity and ultimately the GV strength and size. The magnitude of Cp_{min} increases with lower U^* until the maximum is reached (Fig. 5). For example, for the lower ground clearance (h/D_l = 0·25), the size of the GV at U^* = 8·6 increases by about 65% relative to the low crosswind case (U^* = 17) (Fig. 6). This will have an impact on the number and distribution of particles which are considered within this method. Although for all three cases considered here (U^* = 17, 11, and 8·6), the ingestion fraction of the concrete particles

https://doi.org/10.1017/S0001924000011167 Published online by Cambridge University Press



(a) U^* = 17, (U_∞ = 10ms^{-1})

(b) U^* = 11, (U_∞ = 15ms^{-1})

(c) U^* = 8·6, (U_∞ = 20ms^{-1})

Figure 15. Ingestion position on the fan face as a function of velocity ratio (U^*) for the same size (r_p/r_l = 0·023, r_p = 0·0325m) concrete particle (ρ_p = 2,400kg/m^3). Ground clearance of h/D_l = 0·25. View looking at the fan.

(ρ_p = 2,400kg/m^3) is always close to 1 (Fig. 9(b)), the total number of particles changes from 100 for U^* = 17 to 230 for U^* = 8·6. At a low crosswind (U^* = 17) the Cp_{min} magnitude is moderate (Fig. 5) and for these relatively large concrete particles (r_p/r_l = 0·023) F_{PS}/Q is 16. Nevertheless, about 94% of all particles are ingested across the region φ = 60° to 240° (Fig. 15(a)). The particles on the starboard side region (φ = 60° to 120°) are ingested on the edge of the core inlet whereas particles at φ = 180° to 240° also encompass the fan tip region. This wide radial distribution is caused by the particle-spinner interaction. Some of the particles in the φ = 180° to 240° region were initially directed towards the upper right quadrant (φ = 270° to 360°) but struck and rebound from the spinner and ultimately were ingested at the nominal fan face in the lower right region (φ = 180° to 240°).

https://doi.org/10.1017/S0001924000011167 Published online by Cambridge University Press

For the configuration with U^* = 11 there is a moderate increase in the initial GV suction force (Cp_{min} = –1·5) (Fig. 5) and the F_{PS}/Q = 26 which is similar to the value for U^* = 17. The distribution of particles on the fan face is different with a bias towards the lower right quadrant (φ = 180° to 270°). Again, some of these particles were originally directed into the φ = 30° to 90° region but rebound from the spinner to finally be ingested at φ = 210° to 270°. Due to the slight increase in the initial velocity some of the particles are ingested at a position further from the ground and about 9% of all the particles are ingested in the core region, all of them are in the upper right quadrant.

For a further decrease in the velocity ratio (U^* = 8·6) there is a slight increases the initial suction force acting on the particles (F_{PS}/Q = 30) such that they are now ingested around the full circumference. The radial distribution on the lower half of the fan face (φ = 90° to 270°) is broadly unaffected and is similar to the configuration of U^* = 11.

4.0 CONCLUSIONS

A computational study has been completed to improve the understanding of foreign object ingestion by ground vortex action. The flow field has been investigated with a full scale intake representation for crosswind configurations at a set of ground clearances. The impact of velocity ratio, height-to-diameter ratio, particle density and particle size has been studied. A process was developed for assessing foreign object ingestion for an aero-engine intake under ground vortex conditions. The approach combined an underpinning calculation of the intake and ground vortex flow field with a particle tracking method. The effect of iterative convergence and the computation grid on the ground vortex was evaluated. In addition, the impact of the computational grid on the particle ingestion characteristics was also assessed. The method considers the particle initialisation, tracking and the effect of the particle size and density. The ingestion characteristics for a range of intake ground clearances and crosswind velocities have been assessed in terms of maximum particle size, ingestion fraction and ingestion position within the intake.

The maximum size of an ingested particle depends on the particle density as well as the intake configuration such as velocity ratio and ground clearance. The ingestion characteristics depend on the particle size and density, although it is notable that, in general, the peak ingestion fraction does not coincide with the peak ground vortex strength. Indeed, due to the complexities of the ingestion mechanism the ground vortex suction or vortex circulation are not the sole parameters in determining the peak ingestion fractions.

For a reduction in ground clearance from h/D_l = 0·40 to 0·25, the maximum diameter of an ingested particle increases by up to a factor of around 4·7 which for a steel particle increases the ingested mass from approximately 20g to 2kg. Furthermore, at the lowest ground clearance of h/D_l = 0·25, with a larger particle of low density such as aluminium the maximum ingested debris has a mass of around 10kg. Overall the work presents a generic approach that can be adopted to make quantitative assessments of foreign object ingestion. In particular, the method provides sufficient information on the mass and trajectory of the largest ingested particles to guide design and operability assessments for intake and compression systems.

REFERENCES

1. McCREARY, I. *The Economic Cost of FOD to Airlines*, 2008, Insight SRI.
2. Information paper on French study on automatic FOD detection systems, 2008, EUROCONTROL, Workshop.
3. BRIX, S., NEUWERTH, G. and JACOB, D. The inlet-vortex system of jet engines operating near the ground, August 2000, AIAA Paper 2000-3998.

https://doi.org/10.1017/S0001924000011167 Published online by Cambridge University Press

4. DE SIERVI, F., VIGUIER, H., GREITZER, E. and TAN, C. Mechanisms of inlet vortex formation, *J Fluid Mechanics*, 1982, **124**, pp 173-207.
5. LIU, W., GREITZER, E. and TAN, C. Surface static pressures in an inlet vortex flow field, *J Engineering for Gas Turbines and Power*, 1985, **107**, pp 387-393.
6. SHIN, H., CHENG, W., GREITZER, E. and TAN, C. Inlet vortex formation due to ambient vorticity intensification, *J American Institute of Aeronautics and Astronautics*, 1986, **24**, (4), pp 687-689.
7. SHIN, H., GREITZER, E., CHENG, W., TAN, C. and SHIPPEE, C. Circulation measurements and vertical structure in an inlet vortex flow field, *J Fluid Mechanics*, 1986, **162**, pp 463-487.
8. MURPHY, J. and MACMANUS, D. Ground vortex aerodynamics under crosswind conditions, *Experiments in Fluids*, January 2011, **50**, pp 109-124.
9. MURPHY, J. and MACMANUS, D. Inlet ground vortex aerodynamics under headwind conditions, *Aerospace Science and Technology*, 2011, **15**, pp 207–215.
10. MURPHY, J., MACMANUS, D. and TAYLOR, M. A quantitative study of intake ground vortices, September 2007, ISABE Paper 2007-1209.
11. ZANTOPP, S., MACMANUS, D. and MURPHY, J. Computational and experimental study of intake ground vortices, *Aeronaut J*, December 2010, **114**, pp 769-784.
12. MISHRA, N., MACMANUS, D. and MURPHY, J. Intake ground vortex characteristics, *J Aerospace Eng*, 2012, 226, pp 1387-1400, Proceedings of the Institution of Mechanical Engineers Part G.
13. JERMY, M. and HO, W. Location of the vortex formation threshold at suction inlets near ground planes by computational fluid dynamics simulation, *J Aerospace Eng*, 2008, **222**, pp 393-402, Proceedings of the Institution of Mechanical Engineers Part G.
14. SMITH, T. and COX, P. Debris ingestion by ground vortex into air intake having low ground clearance, August 1969, Rolls-Royce, No IAR 00009.
15. MURPHY, J. Intake Ground Vortex Aerodynamics, PhD thesis, 2008, Cranfield University, UK.
16. GERHOLD, M. and BORE, C. Experimental and theoretical investigation into ingestion of debris into air intakes by vortex action, 1984, British Aerospace report, BAe-KGT-R-GEN-01309.
17. GLENNY, D. Ingestion of debris into intakes by vortex action, 1968, Ministry of Technology, Aeronautical Research Council, CP No 1114.
18. RIDDER, S. and SAMUELSSON, I. An experimental study of strength and existence domain of ground-to-air inlet vortices by ground board static pressure measurements, 1982, Royal Institute of Technology Report KTH AERO TN 62.
19. YADLIN, Y. and SHMILOVICH, A. Simulation of vortex flows for airplanes in ground operations, 2006, AIAA Paper 2006-56.
20. RODERT, L. and GARRETT, F. Ingestion of foreign objects into turbine engine by vortices, 1955, National Advisory Committee for Aeronautics, NACA TN 3330.
21. Advisory Circular: Measurement, construction and maintenance of skid-resistant airport pavement surfaces, 1997, US Department of Transportation No 150/5320-12C.
22. Best practices for the mitigation and control of foreign object damage-induced high cycle fatigue in gas turbine engine compression system airfoils, 2005, NATO Science and Technology Organization, Report RTO-TR-AVT-094.
23. Advisory Circular: Debris hazards at civil airports, 1996, US Department of Transportation No 150/5380-5B.
24. HOXEY, R. and RICHARDS, P. Flow patterns and pressure field around a full-scale building, *J Wind Engineering and Industrial Aerodynamics*, 1993, **50**, pp 203-212.
25. HANSES, F. Surface roughness length, August 1993, US Army Research Laboratory Report ARL-TR-61.
26. MAXEY, M. and RILEY, J. Equation of motion for a small rigid sphere in a nonuniform flow, *Physics of Fluids*, 1983, **26**, pp 883-889.
27. CLIFT, R., GRACE, J. and WEBER, M. *Bubbles, Drops, and Particles*, 1978, Academic Press, London, UK.

https://doi.org/10.1017/S0001924000011167 Published online by Cambridge University Press